LU-TP 20-40
June 2020

Extending the Standard Model by a Dark and a Visible Scalar Singlet

Aram Fatah

Department of Astronomy and Theoretical Physics, Lund University

Bachelor thesis supervised by Johan Rathsman and Jonas Wittbrodt

LUND
UNIVERSITY

Abstract

In this thesis, we extend the Higgs sector of the Standard Model by two scalar singlets and impose a discrete Z_2 symmetry on each of them, under which, both singlets are odd. One of the two scalar singlets will acquire a vacuum expectation value while the other one does not. This leads to one scalar field mixing with the SM-like Higgs field and one stable scalar singlet. Thus, three scalar bosons are present in this model, two of which have couplings to Standard Model particles while the third boson only gains couplings to the other two scalars. This third scalar is stabilized by the unbroken Z_2 symmetry and is a viable dark matter candidate. Using an implementation of the model in MicrOMEGAs, a code for calculating dark matter observables, we study the relic density and compare it to the value observed by the Planck collaboration measurements. We discuss the impact of the model parameters on the relic density and the DM-nucleon scattering cross section and comment on resonance and threshold effects due to the additional scalar.

Populäretenskaplig Text

Den bästa teorin vi har om den subatomära världen kallas för ”Standardmodellen”. standardmodellen beskriver de allra minsta partiklarna och deras interaktioner med varandra genom den elektromagnetiska svaga och starka kraften. Genom åren har Standardmodellen förutspått en rad av olika partiklar som har verifierats experimentellt. År 2012 upptäcktes den allra sista partikeln förutspådd av standardmodellen, den så kallade ”Higgs bosonen”. Standardmodellen är den mest framgångsrika teorin forskare har inom fysik men modellen har stora brister. En av bristerna är att Standardmodellen inte kan beskriva mörk materia som utgör ungefär 80 % av all materia i universum. Mörk materia tros inte interagera med ljus eller partiklarna i Standardmodellen via elektromagnetiska- svaga- eller starka kraften, vilket gör det väldigt svårt att se mörk materia. Dock, interagerar mörk materia med andra partiklar via gravitationskraften och denna effekt kan forskare mäta genom att studera till exempel hur fort stjärnor färdas i omloppsbanan runt galaxer. En hypotes är att den största delen av mörk materia som finns i universum idag skapades kort efter Big Bang och genom att undersöka ljuset från Big Bang kan forskare härleda hur mycket mörk materia som finns i universum.

De senaste decennierna har fysiker försökt komma på en teori som kan beskriva mörk materia. Det finns flera olika utgångspunkter när man utvecklar en teori som ska kunna förklara mörk materia och ett lovande område är att lägga till partiklar i den så kallade Higgs sektorn i Standardmodellen. I denna kandidatuppsats jobbar vi med den så kallade ”The Two Real Singlet Model” vilket innebär att vi lägger till två skalära fält i Standardmodellen, vilket resulterar i en modell med tre ”Higgs Bosoner”. Två av dessa Bosoner interagerar med de andra partiklarna från Standardmodellen och en Boson interagerar bara med de andra Higgs Bosonerna, som är vår mörka partikel och en kandidat för mörk materia. Denna modell ger oss en prognos för hur mycket mörk materia som borde ha skapats efter Big Bang och vi jämför hur detta värde stämmer överens med det hur mycket mörkt materia vi observerar i universum.

Contents

1 Introduction

The existence of Dark Matter (DM) [1] has been well established in observations of radial velocities of galaxies [2, 3], in the mergers of galaxy clusters [4], and it is the dominant part of the matter content in the universe. The DM content in the universe is thought to be set by the amount that was created as a relic after the Big Bang. The early universe was hot and dense, and so lighter particles could annihilate into heavier ones in the thermal bath. This reaction could also go the other way, where the heavier particles would decay or annihilate into the lighter ones and everything was in thermal equilibrium. As the universe expanded, it cooled down and the particles were much more diluted. At a certain temperature there was not enough energy for the lighter particles to annihilate into heavier ones. At some point the annihilation rate, which depends on the number density, temperature and annihilation cross section, of the DM particles became too small and they drop out of the thermal equilibrium. This marks the freeze-out temperature where the density of DM becomes constant and is referred to as the relic density. The magnitude of the relic density depends inversely on how long the DM particle stays in thermal equilibrium. A more strongly interacting DM particle stays in equilibrium longer than a weakly interacting one. The interaction strength of the DM particle can be characterized by its annihilation cross section σ, thus the relic density

$$\Omega_{\mathrm{DM}} h^2 \propto \frac{1}{\langle \sigma v \rangle}, \tag{1}$$

where Ω_{DM} is the dark matter density parameter, h is the current value of the reduced Hubble constant, v is the relative velocity and $< \sigma v >$ is the thermal average of the annihilation cross section DM + DM $\rightarrow$ anything. The magnitude of the relic density is given in units of h^2 to avoid a large uncertainty associated with the Hubble constant.

The most precise measurement of the DM relic density has been performed by the Planck collaboration [5]. The Planck satellite measures tiny differences in the temperature of the cosmic microwave background radiation (CMB). These differences in temperature are a result of variations of density which lead to acoustic waves of baryons, the so called baryonic acoustic oscillations, in the gravitational potential near over dense-regions of DM. The magnitude of the oscillations depends on the density of those regions. By analyzing the CMB spectrum the sizes of these oscillations can be determined and the DM density can be deduced. The most recent measurement of the DM relic density is [5]

$$\Omega_{DM} h^2 = 0.1198 \pm 0.0012. \tag{2}$$

Other experiments directly search for interactions between a DM particle and a nucleon. The XENON1T [6] project is one such experiment that aims to detect rare interactions between a DM particle and a Xenon nucleus. Several tons of liquid Xenon are suspended around three thousand meters below ground to shield the experiment from all avoidable radiation and particles. An interaction of a DM particle with a nucleus will emit electromagnetic radiation that the experiment will detect. After one year of data taking no sign

of DM interactions was discovered. Thus, the XENON1T project have set upper limits on the cross sections of the interactions between a DM particle and a nucleon depending on the mass of the DM particle.

There is no particle in the Standard Model (SM) that is a likely candidate for DM. To obtain a theory of DM a description of the fundamental particles Beyond the SM (BSM) is needed. The DM issue is not the only problem that needs to be dealt with by a model beyond the SM, the problem of baryogenesis cannot be resolved in the SM framework, to name another one.

There are many theories of DM and an overview of possible candidates including sterile neutrinos, axions and supersymmetric particles, as well as a more detailed introduction to DM in general, can be found in Refs. [7, 8]. Extensions of the Higgs sector to obtain a stable, scalar Weakly Interacting Massive Particle (WIMP) are other promising types of DM models. The simplest extension is the addition of a stable scalar singlet to the Higgs sector.

In this thesis, we investigate the Two Real Scalar Singlet Model (TRSM) [9, 10, 11, 12], where the Higgs sector is extended by two scalar singlet fields S and X, and we impose two discrete symmetries Z_2^X and Z_2^S. These are symmetry groups composed of the identity transformation and a changing of the sign, i.e. they are composed of the elements $\{1, -1\}$. Both S and X are odd under their respective symmetries while the rest of the SM fields are even under the symmetries. The addition of another scalar singlet gives rise to more annihilation channels for the DM candidate which increases the annihilation cross section. We study the dark phase where one of the fields does not acquire a vacuum expectation value (vev) and is stabilized by the corresponding unbroken Z_2 symmetry. The remaining field will, however, obtain a non-zero vev and will mix with the SM-like Higgs field and gain couplings to SM particles that are given by the Higgs couplings rescaled by a common factor κ'. The quartic coupling of the Higgs boson and the scalar DM particle gives rise to invisible decays of the Higgs boson, while the Higgs boson couplings themselves are modified compared to those in the SM due to a mixing with the second singlet scalar. There are strong experimental bounds from the ATLAS [13] and CMS [14, 15, 16, 17] on such a mixing as well as on the invisible Higgs boson decay rate [18].The Higgs couplings measurements to gauge bosons and fermions set an important constraint on the magnitude of $\kappa'^2 < 0.12$ [19] while the experimental bounds on BR($h \rightarrow$ invisible) strongly limit possible magnitudes of λ_{hx} and λ_{sx} quartic couplings if the masses of the BSM scalars are below the threshold $m_h/2$. Therefore, we adjust the mixing and the quartic couplings in order to comply with these experimental bounds. We implement the model in the code MicrOMEGAs [20], which is a code for calculating DM observables of any BSM such as the relic density or direct and indirect detection rates of DM.

DM in the TRSM has been previously studied in Refs. [10, 11, 12]. We study regions of parameter space similar to the ones considered in Ref [10]. However, that study predates the discovery of the Higgs boson and significant progress in the search for DM. A more recent paper [11] instead focuses on MeV-scale light mediators. These studies conclude that the TRSM can produce a viable scalar DM candidate.

This thesis is structured as follows. In section 2 the dark phase of the TRSM is introduced and its parameters, couplings and theoretical constraints on the parameter space are discussed. In section 3 we present the region of parameter space under consideration, show the results computed by MicrOMEGAs and discuss how the relic density changes with the masses of our scalar bosons and the choice of parameters. In section 4, we summarize and conclude on our results. In the appendix we show plots for the DM-nucleon cross section.

2 The Two Real Singlet Model

The SM Lagrangian describes the interactions between all the particles in the SM. The part of the SM Lagrangian that is of interest in this thesis is the Higgs sector. In the SM the Higgs potential is of the form

$$V(H) = \lambda_h (H^\dagger H)^2 + \mu_h^2 H^\dagger H, \tag{3}$$

where both parameters λ_h and μ_h^2 are real and H represents the Higgs field which is an isospin doublet scalar field of the form

$$H = \begin{pmatrix} 0 \\ \frac{v+\phi_h}{\sqrt{2}} \end{pmatrix} \tag{4}$$

after electroweak symmetry breaking, where v is the vev with a value of around 246 GeV and ϕ_h is the Higgs particle. When extending the Higgs sector, more fields can be added to the potential, leading to phenomenology different than in the SM. In this work, the Higgs sector of the SM is extended by two real scalar singlet fields S and X.

In the TRSM the scalar potential is of the form [9]

$$\begin{aligned} V = \mu_h^2 H^\dagger H + \mu_x^2 X^2 + \mu_s^2 S^2 + \lambda_h (H^\dagger H)^2 + \lambda_x X^4 \\ + \lambda_s S^4 + \lambda_{hx} X^2 H^\dagger H + \lambda_{sx} S^2 X^2 + \lambda_{hs} S^2 H^\dagger H, \end{aligned} \tag{5}$$

where all the parameters of the potential have to be real due to the hermiticity of the Lagrangian.

After expanding around vevs, the form of the scalar fields is

$$X = \frac{\phi_x + v_x}{\sqrt{2}}, \quad S = \frac{\phi_s + v_s}{\sqrt{2}}, \tag{6}$$

where the $v_{s,x}$ are the vevs and $\phi_{s,x}$ are the weak eigenstates of the fields. Two discrete symmetries Z_2^S and Z_2^X are introduced in this model where the singlet fields transform as, $X \to -X$ and $S \to -S$ respectively. The potential in Eq. (5) does not contain any linear or cubic terms due to the Z_2 symmetries. These symmetries, however, can be spontaneously broken by the fields acquiring a vev which is evident when expanding the potential.

In this work, we study the dark phase where v_x vanishes. Hence, only the Z_2^S symmetry is spontaneously broken, while Z_2^X remains unbroken resulting in a stable singlet ϕ_x, which does not mix with the other two fields. However, the ϕ_h and the singlet ϕ_s will mix such that ϕ_s acquires couplings to the SM particles through the Higgs field. The broken phase where $v_{s,x} \neq 0$ was studied in detail in Ref. [9].

Expanding the potential and setting the first derivative to zero for vanishing fields,

$$\frac{\partial V}{\partial\phi_h \partial\phi_s \partial\phi_x}\Big|_{\phi_h,\phi_s,\phi_x\to 0} = 0, \tag{7}$$

gives the following equations which can be solved for μ_s^2 and μ_h^2,

$$\lambda_h v^3 + \mu_h^2 v + \frac{1}{2}\lambda_{hs} v v_s^2 = 0 \;\Rightarrow\; \mu_h^2 = -\frac{2\lambda_h v^2 + \lambda_{hs} v_s^2}{2}, \tag{8}$$

$$\frac{1}{2}\lambda_{hs} v^2 v_s + \lambda_s v_s^3 + \mu_s^2 v_s = 0 \;\Rightarrow\; \mu_s^2 = -\frac{\lambda_{hs} v^2 + 2\lambda_s v_s^2}{2}. \tag{9}$$

Taking the second derivative of the potential with respect to the fields and using the expressions from Eqs. (8) and (9) gives the mass matrix

$$M^2 = \begin{pmatrix} 2v^2\lambda_h & v v_s \lambda_{hs} & 0 \\ v v_s \lambda_{hs} & 2v_s^2\lambda_s & 0 \\ 0 & 0 & \frac{1}{2}v^2\lambda_{hx} + \frac{1}{2}v_s^2\lambda_{sx} + \mu_x^2 \end{pmatrix} \tag{10}$$

The eigenvalues of M^2 corresponds to the squared physical masses, m_1^2, m_2^2, m_3^2, of the fields. The weak eigenstates ϕ_h, ϕ_s, ϕ_x are related to the mass eigenstates h_1, h_2, h_3 through

$$\begin{pmatrix} h_1 \\ h_2 \\ h_3 \end{pmatrix} = R \begin{pmatrix} \phi_h \\ \phi_s \\ \phi_x \end{pmatrix}, \tag{11}$$

where R is an orthogonal 3×3 rotation matrix,

$$R = \begin{pmatrix} \cos\theta & \sin\theta & 0 \\ -\sin\theta & \cos\theta & 0 \\ 0 & 0 & 1 \end{pmatrix}. \tag{12}$$

The mixing angle is chosen such that one of the mass eigenstates has most of its contribution from the Higgs field. We have the following relations for the weak eigenstates and the mass eigenstates

$$\phi_h = h_1 \cos(\theta) - h_2 \sin(\theta), \tag{13}$$

$$\phi_s = h_1 \sin(\theta) + h_2 \cos(\theta), \tag{14}$$

$$\phi_x = h_3. \tag{15}$$

Since $\phi_x \equiv h_3$ is a mass eigenstate, we will, in the following, use ϕ_x to refer to the DM candidate of mass $m_x = m_3$. The masses of the mass eigenstates h_1 and h_2 are ordered as $m_1 \leq m_2$, the heaviest CP-even state is identified with the Higgs boson with mass 125 GeV. The mass matrix M^2 is diagonalized as

$$\text{diag}(m_1^2, m_2^2, m_x^2) = R^T M^2 R \tag{16}$$

and hence the parameters λ_s, λ_h, λ_{hs} and μ_x can be expressed in terms of the masses and the mixing angles through

$$\begin{aligned} \lambda_s &= \frac{m_1^2 \sin^2(\theta) + m_2^2 \cos^2(\theta)}{2v_s^2}, & \lambda_h &= \frac{m_2^2 \sin^2(\theta) + m_1^2 \cos^2(\theta)}{2v^2}, \\ \lambda_{hs} &= \frac{-(m_1^2 - m_2^2)\cos(\theta)\sin(\theta)}{v v_s}, & \mu_x^2 &= \frac{2m_x^2 - v^2\lambda_{hx} - v_s^2\lambda_{sx}}{2}. \end{aligned} \tag{17}$$

These relations, together with Eqs. (8) and (9) allow us to express the parameters, λ_s, λ_h, λ_{hs}, μ_x^2, μ_s^2 and μ_h^2, in terms of the masses m_1, m_2, m_x, one mixing angle θ, and the vevs v_s and v. We set m_2 to the observed Higgs mass of 125 GeV and the vev v is the Higgs vev equal to 246 GeV leaving the model with seven free parameters

$$m_1\ ,\ \lambda_x,\ m_x,\ \lambda_{sx},\ \lambda_{hx},\ \theta,\ v_s. \tag{18}$$

2.1 Couplings

The interactions that arise from the potential V are triple and quadruple Higgs couplings. The triple Higgs self-couplings are given by

$$V \supset h_a^3[3(2\lambda_h v R_{a1}^3 + 2\lambda_s v_s R_{a2}^3 + \lambda_{hs} R_{a1} R_{a2}[v_s R_{a1} + v R_{a2}])], \tag{19}$$

where $a \in \{1, 2\}$ and R_{ij} are elements of the mixing matrix, Eq. (12). There are no triple self-couplings for ϕ_x due to the Z_2^X symmetry that forbids any couplings with an odd number of ϕ_x. The coupling between two different scalars are given by

$$\begin{aligned} V \supset h_a^2 h_b[6(&\lambda_h v R_{a1}^2 R_{b1} + \lambda_s v_s R_{a2}^2 R_{b2}) - \\ &\lambda_{hs}(v R_{a2}(2R_{12}R_{21} + R_{11}R_{22}) + v_s R_{a1}(R_{12}R_{21} + 2R_{11}R_{22}))], \end{aligned} \tag{20}$$

where $a, b \in \{1, 2\}$ and $a \neq b$. The interactions between ϕ_x and the other two scalars are defined by

$$V \supset \phi_x^2 h_a[\lambda_{hx} v R_{a1} + \lambda_{sx} v_s R_{a2}]. \tag{21}$$

This interaction mediates the annihilation of two ϕ_x into SM particles through an s-channel exchange of $h_{1,2}$ and through t-channel exchange of ϕ_x. The quadruple couplings involving ϕ_x that are relevant for the relic density are

$$V \supset h_a h_b \phi_x \phi_x[\lambda_{hx} R_{a1} R_{b1} + \lambda_{sx} R_{a2} R_{b2}]. \tag{22}$$

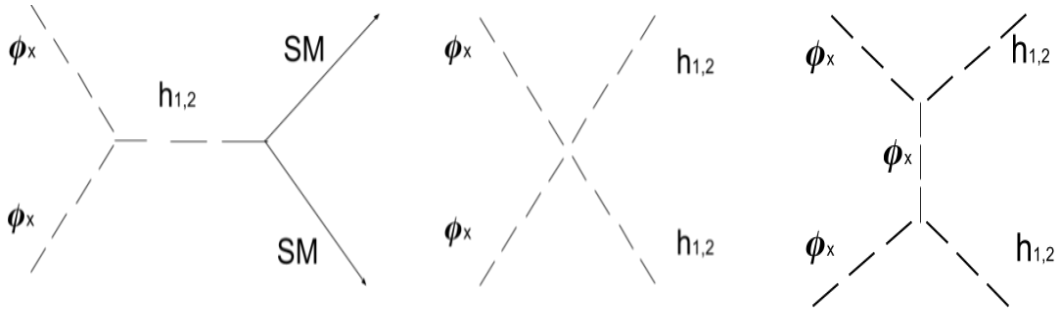

Figure 1: The image to the left shows the annihilation of two ϕ_x particles into SM particles through an s-channel exchange of a scalar boson. The center image shows the contact interaction between ϕ_x and two of the other scalar bosons. The image to the right shows the t-channel exhchange of an ϕ_x

The possible interactions involving ϕ_x are illustrated in Fig. 1.

The λ parameters and the vevs govern the strength of the couplings between the scalar bosons. The value of the mixing angle determines the mixing between the Higgs field and the S field and therefore the couplings between h_1, h_2 and the SM particles. The coupling strengths between the scalar bosons and the SM particles are given by the SM Higgs coupling to the corresponding particle rescaled by a factor

$$\kappa_a = R_{a1}, \tag{23}$$

where $a \in \{1, 2, 3\}$ and R_{a1} are the mixing matrix elements from Eq. (12). As is evident from Eq. (12), ϕ_x does not acquire any coupling since $R_{31} = 0$.

In other phases where $v_x \neq 0$ the h_3 mass eigenstate would also mix with h_1 and h_2 resulting in ϕ_x to pick up some of the SM couplings. However, now X does not have a vev and hence ϕ_x does not mix with the others and so cannot decay into any of the SM fermions and gauge bosons and hence ϕ_x is the dark matter candidate in this phase. Nonetheless, ϕ_x will interact with the other scalar bosons $h_{1,2}$ through the annihilation process shown in Fig. 1, and the strength of these interactions will determine the relic density of h_3.

2.2 Theoretical Constraints

In order for the potential to have a stable vacuum it needs to be bounded from below. In the SM it is enough for the Higgs self-coupling to be positive to ensure boundedness. In the case of the TRSM, since there is more than one field, the potential needs to be bounded from below in all directions of the potential field space in the limit of large field values. In that limit the mass and cubic terms can be ignored since, compared to the quartic terms, they are unimportant at large field values. Hence, the quartic terms are the only ones that need to be constrained. The following constraints on the parameters of the potential ensure its boundedness from below [21]

$$
\begin{aligned}
0 &< \lambda_s, \\
0 &< \lambda_h, \\
0 &< \lambda_x, \\
0 &< \bar{\lambda}_{sx} \equiv \lambda_{sx} + 2\sqrt{\lambda_s \lambda_x}, \\
0 &< \bar{\lambda}_{hs} \equiv \lambda_{hs} + 2\sqrt{\lambda_h \lambda_s}, \\
0 &< \bar{\lambda}_{hx} \equiv \lambda_{hx} + 2\sqrt{\lambda_h \lambda_x}, \\
0 &< \sqrt{\lambda_s \lambda_{hx}} + \sqrt{\lambda_x \lambda_{hs}} + \sqrt{\lambda_h \lambda_{sx}} + \sqrt{\bar{\lambda}_{sx} \bar{\lambda}_{hs} \bar{\lambda}_{hx}}.
\end{aligned}
\tag{24}
$$

As in any theory, the scattering matrix S has to be unitary to maintain meaningful probabilities. This puts constraints on the eigenvalues of the tree-level scattering matrix $|\mathcal{M}^i| < 8\pi$ which have been derived in Ref. [22]. This leads to further constraints on the potential parameters

$$
\begin{aligned}
|\lambda_h| &< 4\pi, \\
|\lambda_{hs}|, |\lambda_{hx}|, |\lambda_{sx}| &< 8\pi, \\
|a_1|, |a_2|, |a_3| &< 16\pi,
\end{aligned}
\tag{25}
$$

where $a_{1,2,3}$ are the real roots of the polynomial $P(x)$ that arises from calculating the eigenvalues of the scattering matrix

$$
\begin{aligned}
P(x) = x^3 + x^2(-12\lambda_h - 6\lambda_s - 6\lambda_x) + x(72\lambda_h(\lambda_s + \lambda_x) \\
- 4(\lambda_{hs}^2 + \lambda_{hx}^2) + 36\lambda_s\lambda_x - \lambda s x^2) \\
+ 12\lambda_h\lambda_{sx}^2 + 24\lambda_{hs}^2\lambda_x + 24\lambda_{hx}^2\lambda_s - 8\lambda_{hs}\lambda_{hx}\lambda_{sx} - 432\lambda_h\lambda_s\lambda_x.
\end{aligned}
\tag{26}
$$

3 Numerical Results

In the phenomenological study we vary the masses m_1 and m_x along with the parameters θ, v_s, λ_x, λ_{hx}, λ_{sx}. The other parameters are determined by the relationships from Eq. (17). Then it is important that the theoretical constraints discussed in the previous section are fulfilled. However, the constraints leave plenty of room to alter the parameters in the region of parameter space under consideration.

As stated earlier, one of the masses m_1 or m_2 is identified with the observed Higgs mass of 125 GeV. We focus on the region of the parameter space where, $m_2 = m_{125} = 125$ GeV, and so h_2 will be referred to as h_{125}, while m_1 and m_x vary in the range

$$
10 \text{ GeV} \leq m_1,\ m_x \leq 120 \text{ GeV}, \tag{27}
$$

while v_s is chosen in the range

$$
100\text{GeV} \leq\ v_s\ \leq 200\text{GeV}. \tag{28}
$$

The remaining free parameters λ_x, λ_{hx} and λ_{sx} are fixed to specific values in the range

$$
0 \leq\ \lambda_x,\ \lambda_{hx},\ \lambda_{sx} \leq 1. \tag{29}
$$

Figures	v_s [GeV]	λ_x	λ_{sx}	λ_{hx}
Fig. 2	150	0.1	0.2	0.09
Fig. 3	150	0.1	0.02	0.09
Fig. 4 a)	150	0.1	0.7	0.035
Fig. 4 b)	150	0.1	0.01	1

Table 1: The table shows values for fixed model parameters for Figs. 2 to 4.

We choose small positive values to, firstly, fulfill the boundedness conditions from Eq. (24) and avoid problems with the unitarity constraints, secondly to ensure that the BR($h_{125} \to \phi_x \phi_x$) remains small. Both the ATLAS and CMS experiments have set an upper limit on the invisible decay branching ratio of the Higgs boson to 24% at a 95 % confidence level. Therefore, we need to choose the potential parameters in such a way that this constraint is satisfied..

The results will be presented in two-dimensional parameter planes of m_1 and m_x. The parameters λ_x, λ_{hx}, λ_{sx} and v_s are set to fixed values and chosen to fullfil the theoretical constraints and reach agreement with the Plank collaboration results, that is, that the relic density does not exceed the measured value. The remaining parameter θ will be set so that the coupling factor κ_{125} from Eq. (23) is near unity since the h_{125} is identified as the Higgs boson. The authors of Ref. [9] used HiggsSignals-2.3.0 [23, 24, 25, 26] to obtain constraints from Higgs measurements on κ_{125} for the TRSM. Their results are based on measurement from the ATLAS [13] and CMS [14, 15, 16, 17] collaborations and it is found that $0.963 < \kappa_{125}$ at 95% confidence level for TRSM. If $\kappa_{125} = 1$ then h_{125} has exactly SM like couplings. Larger values than 1 is not possible in the TRSM since the coupling factors obey the sum rule $\sum_{a=1}^{2} \kappa_a^2 = 1$ due to the orthogonality of the mixing matrix. Thus, we choose $\theta = 1.37 \Rightarrow \kappa_{125} = 0.98$, this grants h_{125} similar couplings as the SM Higgs to the other SM particles. Hence, our choice of κ_{125} should ensure that the experimental constraints set by the ATLAS and CMS results are fulfilled as long as BR($h_{125} \to \phi_x\ \phi_x$) remains small.

In the following, we show the relic density as a function of the two masses m_x and m_1 for four different sets of values for λ_x, λ_{hx}, λ_{sx} v_s, that are given in Table 1. The parameters are chosen so that the theoretical constraints at tree-level are fulfilled throughout the parameter plane spanned by the two masses m_1 and m_x. The parameters λ_x and v_s are not varied since, λ_x only governs the strength of the ϕ_x self couplings and any variation in v_s can be absorbed in variations of λ_{sx}. This is evident from the coupling factor from Eq. (21).

3.1 Relic Density

As mentioned in the introduction, the model is implemented in the code MicrOMEGAs [20], which calculates the relic density of ϕ_x from thermal freeze-out. The model implementation

is done with the help of the Mathematica package SARAH [27] to generate the necessary model files. In the calculation for the relic density, MicrOMEGAs includes all annihilation and coannihilation processes and lists the most important annihilation channels contributing to the relic density. The code also gives the DM-nucleon cross section.

The masses m_1 and m_x are decisive when it comes to what annihilation channels are open and dominating and hence, determine the relic density. If the masses are near an s-channel resonance of an annihilation process where the intermediate scalar boson goes on-shell, the annihilation cross section increases substantially [28]. In our model, there are only two resonances we need to be concerned about, when $m_x \approx m_{125}/2 \approx 62.5$ GeV or $m_x \approx m_1/2$. The annihilation cross section can also be enhanced if m_x reaches a threshold in the final state [28]. An example of this, which we will see in the relic density plots, is when $m_x \geq 80$ GeV $\approx m_W$. Then the annihilation cross section for the process $\phi_x\ \phi_x \to h_{1,125} \to W^+\ W^-$ is enhanced and thus, yields a lower relic density.

By inspection of Eqs. (21) and (22), we notice that the coupling factors for the triple and quadruple couplings between ϕ_x and the other two scalar bosons are dependent on λ_{sx} and λ_{hx}. The cross section for the couplings from Eqs. (21) and (22) are dependent on the coupling factors squared and hence, depending on the strength of these couplings, the cross sections will change subsequently.

3.1.1 Identifying Important Annihilation Channels

In Fig. 2 we can see two regions where the relic density is minimal. One region is the horizontal line at $m_x \approx m_{125}/2$. This line corresponds to the resonance of the annihilation process $\phi_x\ \phi_x \to h_{125} \to$ SM particles. The second region where the relic density is minimal is where $m_x \approx m_1/2$ which is a result of the resonance of $\phi_x\ \phi_x \to h_1 \to$ SM particles. As stated, when the mass of ϕ_x is at such a resonance, the cross section for the interaction is greatly enhanced which results in fewer remaining ϕ_x after freeze-out.

By inspecting Fig. 2, we can see that the plot is split in two parts, as indicated by the dashed line. To the right of the plot where $m_x < m_1$, we can see that the relic density is generally larger than to the left of the line where $m_x > m_1$, ignoring the minimal region at $m_x = m_1/2$. This tendency is because, to the left of the line, the annihilation channel $\phi_x\ \phi_x \to h_1\ h_1$ is kinematically open and hence, the cross section is enhanced. When $m_x < m_1$, the same annihilation channel is closed and so the cross section is reduced, resulting in a larger relic density after freeze-out. This is also why we see an abrupt increase of the relic density along the $m_x = m_{125}/2$ line when m_1 reaches $m_{125}/2$.

We can see from Fig. 2 that the relic density where $m_x \approx 80$ GeV is at a low. As discussed previously, this is because now m_x reaches a threshold in the final state of the annihilation process $\phi_x\ \phi_x \to h_{125} \to W^+\ W^-$. When $m_x \geq 80$ GeV the relic density starts slowly to increase again but still remains low because the channels where the final states consist of the vector bosons W and Z are open, resulting in a increase in the annihilation cross section, and thus, a lower relic density.

We can see that the correct relic density can be reached for any value $m_x < 80$ GeV.

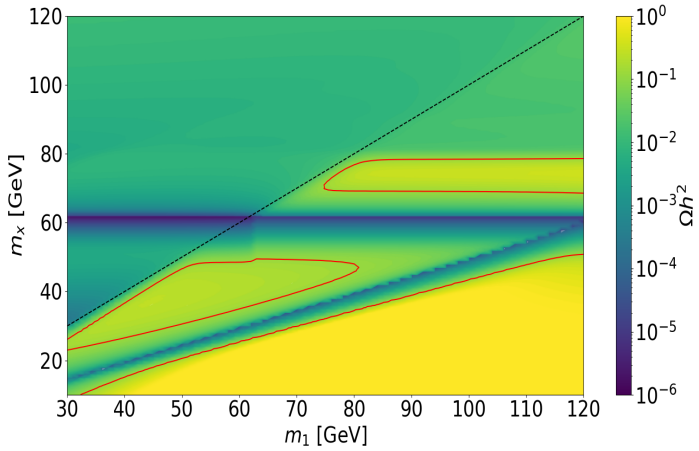

Figure 2: The relic density Ωh^2 where Ω is the relic density parameter and h^2 is the current reduced Hubble constant, is indicated by the colorbar and plotted as a function of the two masses m_1 and m_x. The red lines on the graph marks the regions where the relic density matches the one observed by the Planck satellite, $\Omega_{DM}h^2 = 0.1198 \pm 0.0012$. The remaining parameters are given in Table 1. The dashed line marks the points where $m_x = m_1$.

The regions where the relic density exceeds the observed value are when $m_x < 50$ GeV unless $m_x > m_1$ or $m_x \approx m_1/2$. Regions where the relic density is lower than the observed value are still viable since there can be other sources of DM not accounted for in this model.

3.1.2 Significance of the Parameters

The coupling factors from Eqs. (21) and (22) are important when it comes to understanding the significance of the parameters. When κ_{125} is close to one the coupling factors are

$$\phi_x\ \phi_x\ h_1 \sim \lambda_{sx} v_s \tag{30}$$
$$\phi_x\ \phi_x\ h_{125} \sim \lambda_{hx} v \tag{31}$$
$$\phi_x\ \phi_x\ h_1\ h_1 \sim \lambda_{sx} \tag{32}$$
$$\phi_x\ \phi_x\ h_{125}\ h_{125} \sim \lambda_{hx}. \tag{33}$$

In Fig. 3 we can see the relic density for the same parameter choices as Fig. 2 but λ_{sx} is scaled down by a factor of 10. In Appendix A, we show more plots for different sets of parameter values. Comparing Fig. 3 with Fig. 2, we can see that the effects of the annihilation channels discussed previously still remain. The overall difference between the two results is the magnitude of the relic density at each corresponding point.

In comparison, the overall relic density is lower for a larger value of λ_{sx} since the annihilation cross sections are larger. In the regions where the annihilation channel

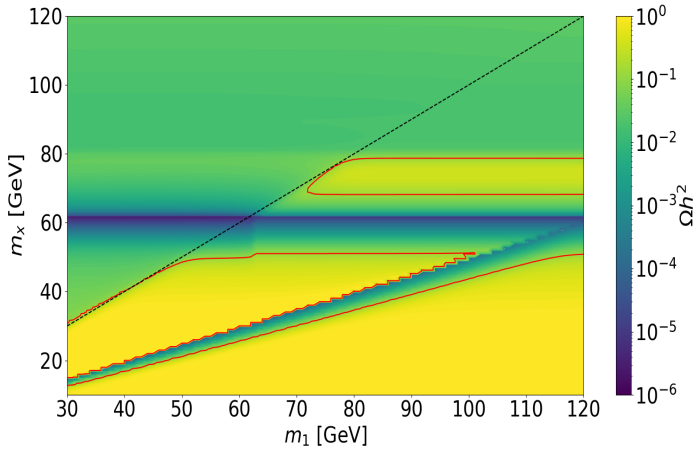

Figure 3: The relic density Ωh^2 where Ω is the relic density parameter and h^2 is the current reduced Hubble constant, is indicated by the colorbar and plotted as a function of the two masses m_1 and m_x. The red lines on the graph marks the regions where the relic density matches the one observed by the Planck satellite, $\Omega_{DM}h^2 = 0.1198 \pm 0.0012$. The remaining parameters are given in Table 1. The dashed line marks the points where $m_x = m_1$.

$\phi_x\ \phi_x \to h_1\ h_1$ is closed and that are far from the h_1 resonance we can see that the value of λ_{sx} has little significance. In the areas close to the $m_x = m_1/2$ resonances or the $m_x > m_1$ threshold the magnitude of the relic density is lower for larger values of λ_{sx}. This is because, even if m_1 is slightly off-shell or the $h_1\ h_1$ threshold is only accessible by involving kinetic energy in the intial state, λ_{sx} is large enough for the cross sections of $\phi_x\ \phi_x \to h_1\ h_1$ to contribute significantly. The parameter λ_{hx} has more significance for the annihilation cross section for $\phi_x\ \phi_x \to h_{125} \to$ SM. In Fig. 4, we can see that when λ_{hx} is large the relic density is low, especially for $m_x > m_{125}/2$.

An interesting effect we can see from Fig. 4 is that when λ_{hx} is large, it has a big impact on the relic density for large values of m_1. Since for the non-resonant process $\phi_x\ \phi_x \to h_{1,125} \to$ SM, λ_{hx} will contribute significantly to the cross section, since h_{125} has a stronger coupling to the SM particles. For large values of λ_{sx}, the effect is not as big, because h_1 has a weaker coupling strength to the SM particles and so, for λ_{sx} to be significant, m_x needs to be near the h_1 resonance or above the $h_1\ h_1$ threshold.

The remaining parameter λ_x does not contribute significantly to the relic density as it is only of importance in the ϕ_x self-couplings.

3.2 DM-nucleon Cross Section

As previously discussed, ϕ_x does not directly couple to SM particles. However, it can interact with nucleons via a t-channel, as illustrated in Fig. 5, interaction with the constituent quarks of a nucleon [10]. The intermediate particle in this interaction is one of the other scalar bosons $h_{1,125}$. In Ref. [10], they derive the cross sections for the interaction

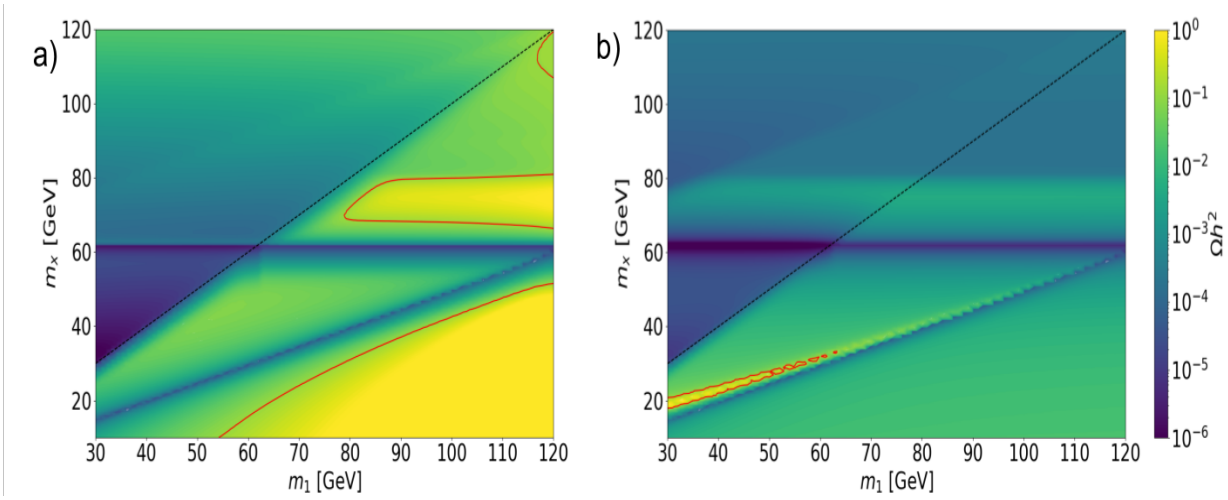

Figure 4: The relic density Ωh^2 where Ω is the relic density parameter and h^2 is the current reduced Hubble constant, is indicated by the colorbar and plotted as a function of the two masses m_1 and m_x. The red lines on the graph marks the regions where the relic density matches the one observed by the Planck satellite, $\Omega_{DM}h^2 = 0.1198 \pm 0.0012$. The remaining parameters are given in Table 1. The dashed line marks the points where $m_x = m_1$.

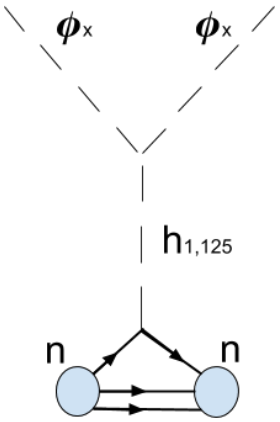

Figure 5: The figure shows the t-channel interaction between ϕ_x and a nucleon where the intermediate particle is one of the scalar bosons h_1 or h_{125}.

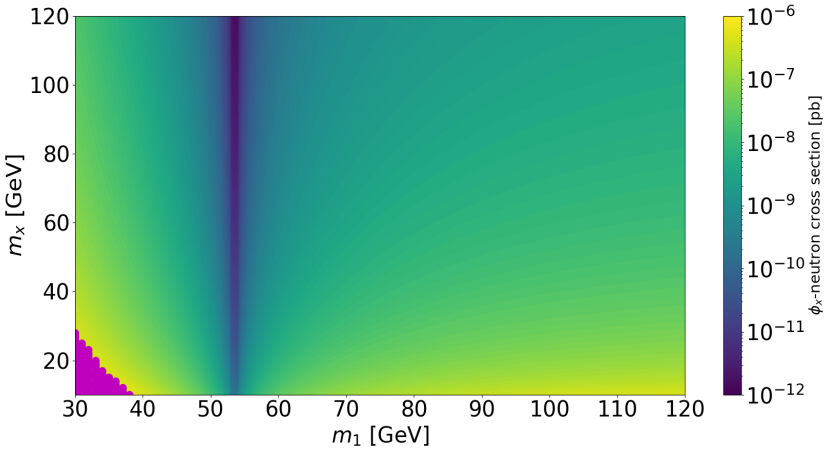

Figure 6: The figure shows the spin independent ϕ_x-neuclon, cross sections, indicated by the colorbar, as a function of the two masses m_x and m_1, for the same choice of parameters as in Fig. 2. The purple area marks the regions where the cross section is greater than the measured upper limit.

displayed in Fig. 5 and show that the cross section is proportional to the quartic mixing parameters $\lambda_{hx,sx}$, the mixing angle θ, as well as the masses of the scalar bosons involved in the interaction, in our notation it reads

$$\sigma_{\phi_x n \to \phi_x n} \sim \frac{\lambda_{hx} \sin\theta}{m_{125}^2} - \frac{\lambda_{sx} \cos\theta}{m_1^2} \tag{34}$$

In Fig. 6 we show the ϕ_x-neutron cross section computed by MicrOMEGAs as a function of the two masses m_x and m_1, for the same choice of parameters as in Fig. 2. We can see that there are some regions excluded by the upper limit on the cross section measured by the XENON1T project [6]. What is interesting is that we see a minimal region where $m_1 \approx 53$ GeV. This minimal region can be seen from Eq. (34). The minimal region arises from an interference effect between the contributions with intermediate h_1 and h_{125} which means, that for some values of the parameters these two contributions will have the same size and opposite signs. Hence, for some values of the parameters the contributions from h_1 and h_{125} will cancel out.

As expected, the cross sections are overall larger for larger values of λ_{sx} and λ_{hx}. Similar to the discussion of the relic density, λ_{hx} is more significant than λ_{sx} since h_{125} is more strongly coupled to quarks than h_1 and hence has a larger impact on the cross section.

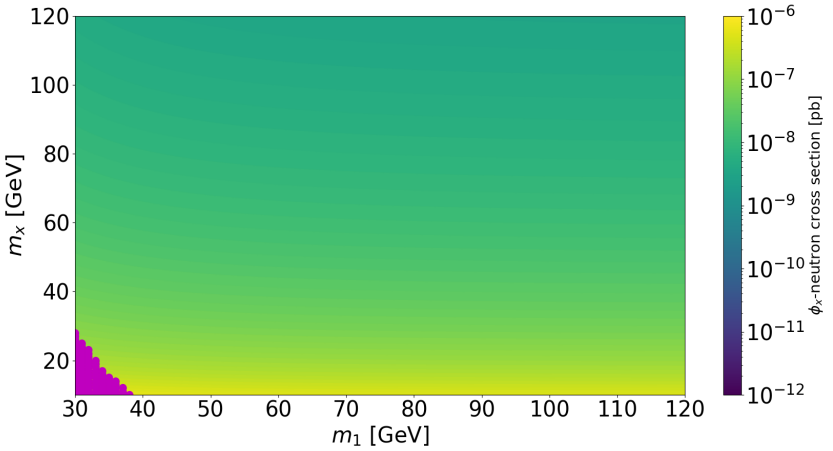

Figure 7: The figure shows the spin independent ϕ_x-neucleon cross sections, indicated by the colorbar, as a function of the two masses m_x and m_1, for the same parameters as in Fig. 3.The purple area marks the regions where the cross section is greater than the measured upper limit.

4 Conclusion

In this thesis, we have studied the dark phase of the two real singlet model (TRSM) where one of the two imposed Z_2 symmetries remains unbroken. This lead to the presence of two scalar bosons $h_{1,2}$, one of which is identified with the Higgs boson with an observed mass of 125 GeV and one stable scalar boson ϕ_x that is a dark matter candidate. We have derived the couplings in the scalar couplings and discussed the theoretical constraints on the model parameters. Using the SARAH package, the model was implemented in MicrOMEGAs which calculated the relic density and nucleon cross section of the dark matter candidate.

We identified $h_2 = h_{125}$ with the observed Higgs boson. Since the singlet field mixes with the SM-like Higgs field, h_1 gains couplings to SM particles, while ϕ_x only couples to the other scalar bosons. These cubic and quadruple scalar couplings, together with the masses m_x and m_1 have a large impact on the relic density. We found that the masses not only determine which annihilation channels for ϕ_x are open but can also lead to large enhancements of the annihilation cross section through resonance and threshold effects. Furthermore, we have discussed the impact of the quartic couplings λ_{sx} and λ_{hx} on the annihilation cross section and found that λ_{sx} is more important near the h_1 resonance and when the $\phi_x\phi_x \to h_1h_1$ channel is open, while λ_{hx} is especially relevant in the non-resonant region.

The ϕ_x nucleon cross section depends on the mixing parameters $\lambda_{hx,sx}$. For the region of parameter space we chose to investigate, the ϕ_x-nucleon cross section is mostly below the upper limit determined by the XENON1T project.

We conclude that a two scalar singlet extension of the Higgs sector is a feasible dark matter model if one of the scalars does not acquire a vacuum expectation value. For the region of parameter space we investigated, the model could predict a relic density which matches the value the observed by the Planck collaboration. There were plenty of regions in the parameter space where the relic density was well below the measured value and hence, the model allows for sources of dark matter in the universe. The region of parameter space we studied allows for both invisible and semi-invisible decays of h_{125} that could be used to look for a dark matter candidate at the LHC in the future.

Acknowledgements

I would like to thank my supervisor Jonas Wittbrodt for guiding me through this thesis and providing me with good explanations and discussions, and also for helping me improve my writing skills. I would also like to express thanks to Astrid Ordell who spent time helping me when Jonas was not available.

5 Appendix A

The graphs displayed in Figs. 8 and 9 shows the ϕ_x-neutron cross sections for the same choice of parameters as in Fig. 4. The ϕ_x-proton cross sections look identical.

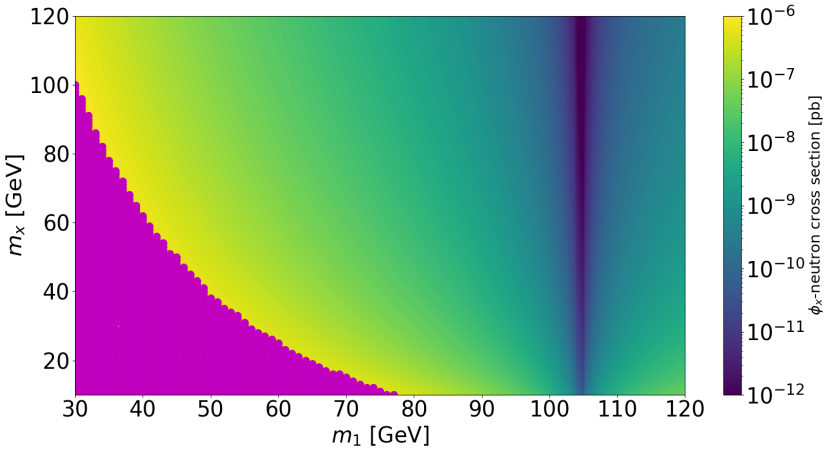

Figure 8: The figure shows the spin independent ϕ_x-neutron cross sections, indicated by the colorbar, as a function of the two masses m_x and m_1, for the same parameters as in Fig. 4 a).The purple area marks the regions where the cross section is greater than the measured upper limit.

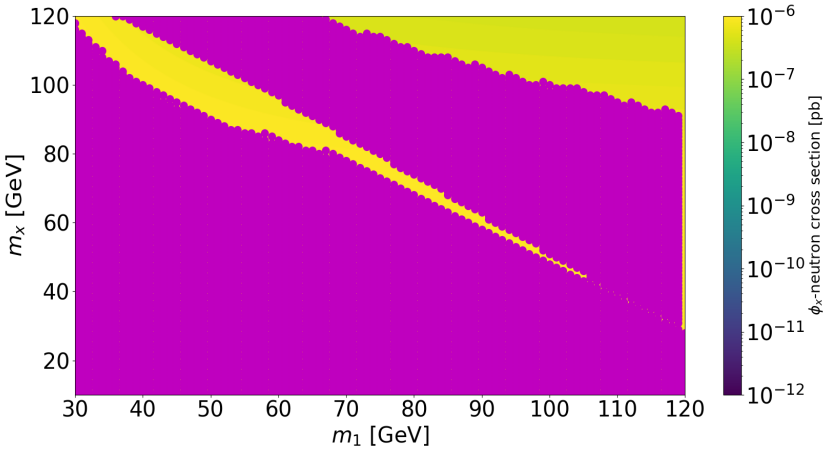

Figure 9: The figure shows the spin independent ϕ_x-neucleon cross sections, indicated by the colorbar, as a function of the two masses m_x and m_1, for the same parameters as in Fig. 4 b).The purple area marks the regions where the cross section is greater than the measured upper limit.

References

[1] F. Zwicky. "On the Masses of Nebulae and of Clusters of Nebulae". In: 86 (Oct. 1937), p. 217. DOI: 10.1086/143864.

[2] F. Zwicky. "Republication of: The redshift of extragalactic nebulae". In: *General Relativity and Gravitation* 41.1 (2009), pp. 207–224. ISSN: 00017701. DOI: 10.1007/s10714-008-0707-4.

[3] R. H. Sanders. "The Published Extended Rotation Curves of Spiral Galaxies: Confrontation with Modified Dynamics". In: *The Astrophysical Journal* 473.1 (Dec. 1996), pp. 117–129. ISSN: 1538-4357. DOI: 10.1086/178131. URL: http://dx.doi.org/10.1086/178131.

[4] Douglas Clowe et al. "A Direct Empirical Proof of the Existence of Dark Matter". In: *The Astrophysical Journal* 648.2 (2006), pp. L109–L113. ISSN: 0004-637X. DOI: 10.1086/508162. arXiv: 0608407v1 [arXiv:astro-ph].

[5] "Planck 2018 results. VI. Cosmological parameters". In: *Astronomy & Astrophysics* (2020). ISSN: 0004-6361. DOI: 10.1051/0004-6361/201833910. arXiv: 1807.06209.

[6] E. Aprile et al. "Dark Matter Search Results from a One Ton-Year Exposure of XENON1T". In: *Physical Review Letters* 121.11 (2018), pp. 1–8. ISSN: 10797114. DOI: 10.1103/PhysRevLett.121.111302. arXiv: arXiv:1805.12562v2.

[7] Gianfranco Bertone, Dan Hooper, and Joseph Silk. "Particle dark matter: Evidence, candidates and constraints". In: *Physics Reports* 405.5-6 (2005), pp. 279–390. ISSN: 03701573. DOI: 10.1016/j.physrep.2004.08.031. arXiv: 0404175 [hep-ph].

[8] Jonathan L. Feng. "Dark Matter Candidates from Particle Physics and Methods of Detection". In: *Annual Review of Astronomy and Astrophysics* 48.1 (2010), pp. 495–545. ISSN: 0066-4146. DOI: 10.1146/annurev-astro-082708-101659. arXiv: 1003.0904.

[9] Tania Robens, Tim Stefaniak, and Jonas Wittbrodt. "Two-real-scalar-singlet extension of the SM: LHC phenomenology and benchmark scenarios". In: *European Physical Journal C* 80.2 (2020), pp. 1–34. ISSN: 14346052. DOI: 10.1140/epjc/s10052-020-7655-x. arXiv: 1908.08554.

[10] Abdessamad Abada, Djamal Ghaffor, and Salah Nasri. "Two-singlet model for light cold dark matter". In: *Physical Review D - Particles, Fields, Gravitation and Cosmology* 83.9 (2011), pp. 1–30. ISSN: 15502368. DOI: 10.1103/PhysRevD.83.095021. arXiv: arXiv:1101.0365v1.

[11] A. Arhrib and M. Maniatis. "The two-real-singlet Dark Matter model". In: *Physics Letters, Section B: Nuclear, Elementary Particle and High-Energy Physics* 796 (2019), pp. 15–19. ISSN: 03702693. DOI: 10.1016/j.physletb.2019.07.023. arXiv: 1807.03554.

[12] Peter Athron et al. “Status of the scalar singlet dark matter model”. In: *European Physical Journal C* 77.8 (2017), pp. 1–19. ISSN: 14346052. DOI: 10.1140/epjc/s10052-017-5113-1. arXiv: 1705.07931.

[13] M. Aaboud et al. “Combined measurements of Higgs boson production and decay using up to 80 fb(-1) of proton-proton collision data at s = 13 TeV collected with the ATLAS experiment”. In: *48* (2020). DOI: 10.1103/PhysRevD.101.012002/apsxml.

[14] Cms Collaboration. “CMS Physics Analysis Summary”. In: *Cms Pas Bph-10-002* 22.July (2013), pp. 0–5. ISSN: 1098-5530. DOI: CMS-PAS-HIG-13-032. arXiv: /inspirehep.net/record/1260835/files/SUS-12-030-pas.pdf [Mssm, P. (2013). CMS Physics Analysis Summary. Retrieved from https:]. URL: http://cms-project-physics.web.cern.ch/cms-project-physics/public/HIG-07-001-pas.pdf.

[15] Cms Collaboration. “CMS Physics Analysis Summary”. In: *Cms Pas Bph-10-002* 31.July (2013), pp. 0–5. ISSN: 1098-5530. DOI: CMS-PAS-HIG-13-032. arXiv: /inspirehep.net/record/1260835/files/SUS-12-030-pas.pdf [Mssm, P. (2013). CMS Physics Analysis Summary. Retrieved from https:]. URL: http://cms-project-physics.web.cern.ch/cms-project-physics/public/HIG-07-001-pas.pdf.

[16] A. M. Sirunyan et al. “Evidence for the Higgs boson decay to a bottom quark–antiquark pair”. In: *Physics Letters, Section B: Nuclear, Elementary Particle and High-Energy Physics* 780 (2018), pp. 501–532. ISSN: 03702693. DOI: 10.1016/j.physletb.2018.02.050. arXiv: 1709.07497.

[17] Cms Collaboration. “CMS Physics Analysis Summary”. In: *Cms Pas Bph-10-002* 48.July (2013), pp. 0–5. ISSN: 1098-5530. DOI: CMS-PAS-HIG-13-032. arXiv: /inspirehep.net/record/1260835/files/SUS-12-030-pas.pdf [Mssm, P. (2013). CMS Physics Analysis Summary. Retrieved from https:]. URL: http://cms-project-physics.web.cern.ch/cms-project-physics/public/HIG-07-001-pas.pdf.

[18] G. Aad et al. “Measurements of the Higgs boson production and decay rates and coupling strengths using pp collision data at

$$\sqrt{s} = 7$$

s = 7 and 8 TeV in the ATLAS experiment”. In: *The European Physical Journal C* 76.1 (Jan. 2016). ISSN: 1434-6052. DOI: 10.1140/epjc/s10052-015-3769-y. URL: http://dx.doi.org/10.1140/epjc/s10052-015-3769-y.

[19] G. Aad et al. “Constraints on new phenomena via Higgs boson couplings and invisible decays with the ATLAS detector”. In: *Journal of High Energy Physics* 2015.11 (Nov. 2015). ISSN: 1029-8479. DOI: 10.1007/jhep11(2015)206. URL: http://dx.doi.org/10.1007/JHEP11(2015)206.

[20] G. Belanger, F. Boudjema, and A. Pukhov. "MicrOMEGAs: A package for calculation of dark matter properties in generic model of particle interaction". In: *Proceedings of the 2011 Theoretical Advanced Study Institute in Elementary Particle Physics, TASI 2011: The Dark Secrets of the Terascale* (2013), pp. 739–790. DOI: 10.1142/9789814390163_0012.

[21] Kristjan Kannike. "Vacuum stability of a general scalar potential of a few fields". In: *The European Physical Journal C* 76.6 (June 2016). ISSN: 1434-6052. DOI: 10.1140/epjc/s10052-016-4160-3. URL: http://dx.doi.org/10.1140/epjc/s10052-016-4160-3.

[22] Jonas Wittbrodt. "Exploring Models of Electroweak Symmetry Breaking at the LHC and Beyond". In: (2019). DOI: 10.3204/PUBDB-2019-03809.

[23] Oscar STAL and Tim STEFANIAK. "Constraining extended Higgs sectors with HiggsSignals". In: (2018), p. 314. DOI: 10.22323/1.180.0314. arXiv: 1310.4039.

[24] Philip Bechtle et al. "HiggsSignals: Confronting arbitrary Higgs sectors with measurements at the Tevatron and the LHC". In: *European Physical Journal C* 74.2 (2014), pp. 1–40. ISSN: 14346052. DOI: 10.1140/epjc/s10052-013-2711-4. arXiv: 1305.1933.

[25] Philip Bechtle et al. "Probing the Standard Model with Higgs signal rates from the Tevatron, the LHC and a future ILC". In: *Journal of High Energy Physics* 2014.11 (2014). ISSN: 10298479. DOI: 10.1007/JHEP11(2014)039. arXiv: 1403.1582.

[26] *higgssignals @ gitlab.com*. URL: https://gitlab.com/higgsbounds/higgssignals.

[27] *home @ gitlab.in2p3.fr*. URL: https://gitlab.in2p3.fr/goodsell/sarah/-/wikis/home.

[28] Kim Griest and David Seckel. "Three exceptions in the calculation of relic abundances". In: *Physical Review D* 43.10 (1991), pp. 3191–3203. ISSN: 05562821. DOI: 10.1103/PhysRevD.43.3191.